OPTIONS FOR SCALED EXPERIMENTS FOR HIGH TEMPERATURE LIQUID SALT AND HELIUM FLUID MECHANICS AND CONVECTIVE HEAT TRANSFER

THERMAL HYDRAULICS

KEYWORDS: *liquid and molten salts, very high-temperature reactors, scaled experiments*

PHILIPPE M. BARDET and PER F. PETERSON*
University of California, Nuclear Engineering Department, Berkeley, California 94720

Received October 11, 2006
Accepted for Publication June 29, 2007

Liquid fluoride salts and helium have desirable properties for use as working fluids for high-temperature (500 to 1000°C) heat transport in fission and fusion applications. This paper presents recent progress in the design and analysis of scaled thermal-hydraulic experiments for fluid mechanics and convective heat transfer in liquid salt and helium systems. It presents a category of heat transfer fluids and a category of light mineral oils that can be used for scaled experiments simulating convective heat transfer in liquid salts. By optimally selecting the length, velocity, average temperature, and temperature difference scales of the experiment, it is possible to simultaneously match the Reynolds, Froude, Prandtl, and Grashof numbers in geometrically scaled experiments operating at low-temperature, reduced length, and velocity scales. Mechanical pumping power and heat input are reduced to ~1 to 2% of the prototype power inputs. Helium fluid mechanics and heat transfer likewise can be simulated by nitrogen following the same procedure. The resulting length, velocity, temperature, and power scales for simulating helium are quite similar to those for the liquid salts, and the pressure scale is reduced greatly compared to the prototypical pressure scale. Steady state and transient heat transfer to a steel and graphite structure can be reproduced with moderate distortion using Pyrex and high-thermal-conductivity epoxies, respectively. Thermal radiation heat transfer cannot be reproduced, so the use of these simulant fluids is limited to those cases where radiation heat transport is small compared to convective heat transport, or where corrections for thermal radiation heat transfer can be introduced in models using convective heat transfer data from the simulant fluids. Likewise for helium flows, compressibility effects are not reproduced.

I. INTRODUCTION

High-pressure helium and liquid fluoride salts are two of the heat transfer fluids being considered for use in the production of hydrogen and electricity in the Generation IV Very High Temperature Reactor (VHTR). This paper presents methods to select simulant fluids and scaling parameters for experiments to reproduce fluid mechanics and heat transfer phenomena for those high-temperature fluids at reduced temperature, pressure, length, and power scales.

Liquid fluoride salts, as pictured in Fig. 1, potentially have large benefits for use in high-temperature heat transport in fission and fusion energy systems because of their very low vapor pressures at high temperatures. Liquid fluoride salts are created using the most electronegative element in existence, fluorine, combined with highly electropositive elements like lithium, sodium, potassium, beryllium, and zirconium, creating highly stable compounds. Excellent corrosion resistance has been demonstrated with high-nickel alloys, graphite, and carbon composites. Liquid salts have a high volumetric heat capacity ρC_p, significantly larger than high-pressure helium and liquid metals (Table I), giving heat transport and pumping power characteristics similar to pressurized water. They have very high boiling temperatures, typically above 1300°C, and relatively high melting temperatures (320 to 500°C), necessitating the use of heat tracing and drain tanks for freezing control. The high chemical inertness and low vapor pressure provide good safety

*E-mail: peterson@nuc.berkeley.edu

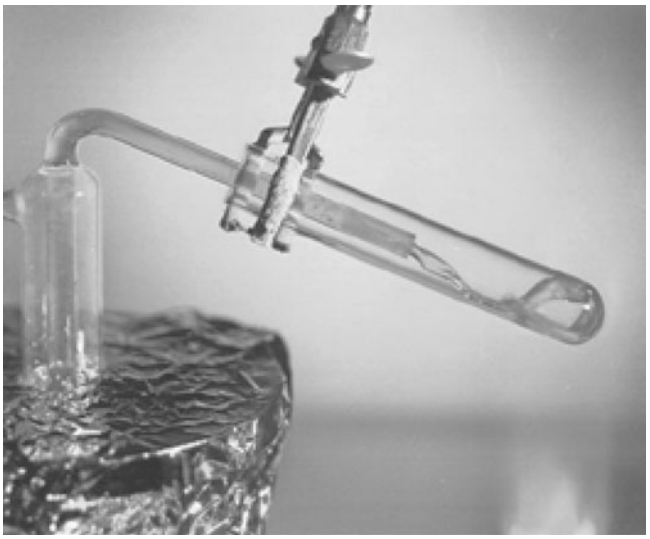

Fig. 1. Liquid flibe (Li_2BeF_4) in air flowing into a fused silica test tube (credit ORNL).

characteristics, eliminating the rapid stored energy release possible with high-pressure gases, high-pressure volatile liquids like water, and chemically reactive coolants like sodium. Liquid salts are dielectric and transparent and are compatible at high temperatures with window materials like sapphire, enabling visual in-service inspection of submerged structures in reactor systems as is performed in water-cooled reactor vessels.

Liquid salts were originally developed in the 1950s and 1960s as solvents for liquid fuels for the Aircraft Nuclear Propulsion Program and the Molten Salt Breeder Reactor Program.[1] These programs operated various salt test loops for several hundred-thousand hours and produced more than 1000 technical reports on technical developments for large centrifugal pumps, heat exchangers, materials, and system design. (The chemical industry also uses a variety of liquid salts in heat transport systems but at somewhat lower temperatures.) Thermophysical properties of several of the liquid salts have been studied extensively, although the thermal conductivity is the most challenging to measure and has the greatest uncertainty.[2]

With this extensive technical database, over the last two decades liquid salts have been studied for use as high-temperature coolants for fusion blankets.[3,4] More recently, they have been proposed for use in the 50-MW(thermal) intermediate heat transfer loop for thermochemical hydrogen production in the Next Generation Nuclear Plant[5] (NGNP). For the NGNP intermediate loop application for hydrogen production, liquid salts provide greatly reduced pumping power and much smaller piping diameter than would high-pressure helium. Likewise, they have attractive characteristics for cooling prismatic and pebble fuel of the same type used in gas-cooled reactors, resulting in their study as a primary coolant for the Advanced High Temperature Reactor[6] (AHTR). In the AHTR application, the improved heat transport capability of liquid salt, compared to high-pressure helium, allows reactor power to be increased by a factor of 4 compared to helium cooling and allows the reactor to operate at low pressure in a pool configuration.

Gas-cooled reactors, like the NGNP and the General Atomics gas turbine–modular helium reactor (GT-MHR), use high-pressure helium as the primary coolant. Because helium can be used at high temperatures, high efficiency can be attained for electricity production and thermochemical hydrogen production. Helium and helium-nitrogen mixtures are also the heat transfer fluids of choice for power conversion systems for high-temperature electricity production, such as for the NGNP, AHTR, Molten Salt Reactor (MSR), and future fusion energy systems.

For these reactors, high-temperature convective heat transport phenomena with liquid salts and high-pressure helium will play important roles in the steady-state, transient, and accident response. Ideally, these fluid mechanics and convective heat transport phenomena can be studied using scaled experiments with reduced size, temperature, and power. Data from scaled experiments can then be used to validate analytical models and benchmark numerical codes. This paper identifies light mineral oils and heat transfer fluids that have desirable properties for simulation of the behavior of high-temperature liquid salts, and nitrogen or air to simulate high-temperature and high-pressure helium. Indeed, when used in a reduced-scale facility where fused silica or Pyrex simulates the metallic structures, these fluids allow the simulation of the liquid salt and helium fluid mechanics and convective heat transfer at reduced size, temperature, and pressure and greatly reduced pumping and thermal power inputs.

Because the scaled experiments operate at relatively low temperatures, radiative heat transfer is not reproduced. This limits the application of these fluids to systems where radiative heat transfer is small compared to convective heat transfer, or where corrections for the effects of radiation heat transfer can be calculated analytically or measured experimentally. Section III discusses radiation heat transfer and the potential resulting distortions in experimental results.

The oil refractive index nearly matches that of fused silica and Pyrex, which permits the use of flow visualization methods such as laser particle velocimetry. Conveniently, the thermal properties of these transparent container materials match, with modest distortion, the scaled thermal properties of typical nickel alloys used as container materials for liquid fluoride salts. Likewise, here it is also shown that low-temperature, intermediate-pressure nitrogen can be used to match heat transfer and fluid mechanics phenomena for high-pressure, high-temperature helium with similar length

TABLE I

Approximated Liquid Salt Thermophysical Properties*

	T (°C)	ρ (kg/m^3)	C_P (kJ/kg·K)	ρC_P (kJ/m^3·K)	ν (m^2/s × 10^6)	σ (N/m × 10^3)	k (W/m·K)	Pr
Flibe	700	1940	2.42	4690	2.9	179	1	13.5
NaF-ZrF_4	700	3140	1.17	3680	1.6	No data	0.49	12.2
NaF-$NaBF_4$	700	1750	1.51	2640	0.5	77	0.40	3.3
Flinak	700	2020	1.89	3810	1.4	No data	0.92	5.9
Helium	700	3.7	5.2	19	12.4		0.36	0.66
Water	300	720	5.74	4130	0.13	16.7	0.54	0.97
Sodium	550	820	1.27	1040	0.28	No data	62.0	0.004

*From Ref. 2. The salt compositions are in mol percent: Flibe (66 mol% LiF–34 mol%BeF_2); NaF-ZrF_4 (50-50); NaF-$NaBF_4$ (8-92); and Flinak, LiF-NaF-KF (46.5-11.5-42). Shown for reference are values for 7.5 MPa helium, 7.5 MPa saturated water, and atmospheric sodium.

and velocity scales. Because the sound speed does not scale, helium experiments are limited to cases where compressibility effects are small.

For systems where only fluid mechanics are of interest, water can be used as a simulant fluid for liquid salts and can match Reynolds and Froude numbers in experiments with similar length and velocity scales.

II. OVERVIEW

To select scaling parameters for experiments for fluid mechanics or convective heat transport, one can normalize the governing differential equations for mass, momentum, and energy conservation, and their boundary and initial conditions, using length, velocity, time, and temperature scales selected to give nondimensional velocity, position, temperature, and pressure variables with magnitudes of order unity.[7] From the momentum differential governing equation with a forced-convection velocity scale U, the Strouhal number ($\mathrm{St} \equiv \tau U/L$), Reynolds number ($\mathrm{Re} \equiv Ul/\nu$), and Froude number ($\mathrm{Fr} \equiv U^2/gL$) emerge. St compares the transient phenomena timescale τ with the fluid transit timescale $\tau_{conv} \equiv L/U$, where L and U are the system length and velocity scales. Re represents the ratio of inertia forces to viscous forces, where ν is the kinematic viscosity. Fr represents the ratio of inertia forces to gravitational forces, where g is the acceleration of gravity. If forced-convection heat transport is of interest, nondimensionalization of the energy equation gives the Prandtl number, $\mathrm{Pr} \equiv \nu/\alpha$, where α is the thermal diffusivity. Pr represents the ratio of viscous diffusion of momentum to the thermal diffusion of heat. Heat transfer is characterized by the Nusselt number Nu. When the flow is driven by buoyancy, the Grashof number, $\mathrm{Gr} \equiv gL^3\beta\Delta T/\nu^2$, where β is the coefficient of thermal expansion and ΔT is the temperature difference scale, replaces the Reynolds number when the energy and momentum equations are nondimensionalized. Gr represents the ratio of buoyant to viscous forces.

To take into account the variation of fluid properties with temperature, it is convenient to introduce the dimensionless numbers $\beta\Delta T$, $\gamma\Delta T$, and $\kappa\Delta T$. These represent the fractional change of density, viscosity, and thermal conductivity between high- and low-temperature regions in the system. The physical property χ (β, γ, or κ) is defined as $\chi = -(1/\phi)(\partial\varphi/\partial T)|_{T_0, P_0}$, where φ is the thermophysical property, density ρ, viscosity μ, or thermal conductivity k.

Finally, the nondimensional differential boundary conditions lead to two dimensionless groups. For interface hydrodynamics, the Weber number arises; $\mathrm{We} \equiv \rho U^2 L/\sigma$, where σ is the surface tension and ρ is the fluid density. For heat transfer a modified Biot number arises, defined in this paper as $\mathrm{Bi}^* \equiv k \cdot l/\lambda \cdot L$, where k and λ are the fluid and solid thermal conductivities, respectively, and L and l are the fluid and solid length scales. Bi^* describes the continuity of heat transfer at the liquid-solid interface, in the absence of thermal radiation.

In the following sections the subscripts m and p designate the scaled model and the prototype, respectively. First, thermal radiation effects are analyzed; then, the general scaling approach for convective heat transfer is presented for a liquid and for an ideal gas; and then, a concise list of potential candidate fluids to simulate high-temperature liquid salts and helium, and candidate container materials, is introduced. The last part of this paper provides representative values of the major scaling parameters for experiments to simulate high-temperature liquid salts and helium.

III. THERMAL RADIATION

Radiation is a complex phenomenon that depends on space and time and is also spectral and directional.

Furthermore, radiative heat transfer depends on the system geometry, and absorptivity, emissivity, etc. These are functions of wavelength, temperature, and chemical composition and, as a consequence, are difficult to accurately characterize experimentally.[8] To determine if radiation is relevant to a heat transfer problem and should even been considered, its first-order effects are commonly considered, and simplifying assumptions are employed. Those assumptions include, but are not limited to, gray surfaces with uniform emissivity, black surfaces, radiatively nonparticipating and optically thin media, and opaque media.

In the case of nonparticipating fluid, i.e., a transparent fluid where absorption, emission, and scattering are negligible, fluid governing equations are unchanged, and radiation transfer is simply a boundary condition at solid surfaces. If the temperature is prescribed at the wall, radiation and convection are uncoupled and can be treated separately. If the net heat flux is prescribed, radiation will change the wall temperature, and radiative and convective heat transfer must be treated simultaneously. Several studies of this last case have been conducted for fully developed laminar convection in simple geometries.[8] Scaling rules have also been derived to determine the relative importance of radiation and convection.[9]

When a fluid is participating, then the governing equations for continuity and momentum are unchanged (radiation pressure is negligible), but the energy equation includes coupling of radiation and convection by subtracting the divergence of the radiation flux term (radiation energy storage is also negligible). Depending on the pressure, temperature, and optical thickness of the translucent fluid, radiation can impede or enhance the convective heat transfer.[10,11] For moderate pressures in steam, the combined Nusselt number can be estimated by the sum of solely radiative and solely convective Nusselt numbers.

The scaled experiments described here operate at relatively low temperatures where radiative heat transfer is small. Conversely, helium and liquid salt applications involve temperatures where thermal radiation heat transfer has the potential to be significant. Therefore, in all cases the potential effects of thermal radiation must be considered in the design of experiments. Experimental data from the use of low-temperature simulant fluids can be used only when thermal radiation effects are either small and can be neglected or where corrections can be applied to account for thermal radiation effects.

Helium is a monoatomic gas, and its contributions to thermal radiation result from electronic transitions, which are negligible for temperatures less than several thousand degrees Kelvin.[12] Therefore, helium can be considered transparent for the temperatures and pressures of interest for nuclear applications (unlike water vapor and carbon dioxide, which have significant absorption in the visible and infrared spectra). Radiative heat transfer then occurs only between solid surfaces. The relative influence of radiation with respect to convection can be estimated using the scaling rules referred to earlier.[9] In addition, in cases of flow in heat transfer channels, it is commonly the case that surfaces that view each other have similar temperatures, so the net radiation heat transfer can be small compared to convective heat transfer. In these cases radiative heat transfer can be neglected, or experimental data can be corrected to include effects of radiation.

Simple halide salts (those with no chromophores, i.e., those with group I, II, and Zr cations, and without transition metals that provide colors), such as the liquid fluoride salts, are transparent in the visible and near-infrared spectrums. Halide salts have sufficiently high transparency that they are commonly used for infrared windows, where their transparency can be higher than oxides like quartz.

Unfortunately, data and modeling for the effects of infrared absorption on liquid salt heat transfer are not well developed. Measurements of liquid salt infrared absorption were made in the process of measuring the salt thermal conductivity,[13,14] but actual data were not reported before the MSR program at Oak Ridge National Laboratory (ORNL) was ended. At present, the only data available to the authors are for salt-based glasses and are used here to estimate the effects of radiation in liquid salts.

Figure 2 shows transmission as a function of wavelength of infrared radiation through 4-mm-thick samples of several glasses.[15] Also shown in Fig. 2 is the blackbody emissive power for surfaces at 600 and 800°C. For the BeF_2-based glass, the cutoff wavelength for infrared absorption is located near the peak of the emissive power for these two temperatures. Conversely, for heavier elements like ZrF_4 the glass can be transparent up to much longer wavelengths.

To the right of the infrared cutoff wavelength for a given salt, radiation heat transfer becomes unimportant

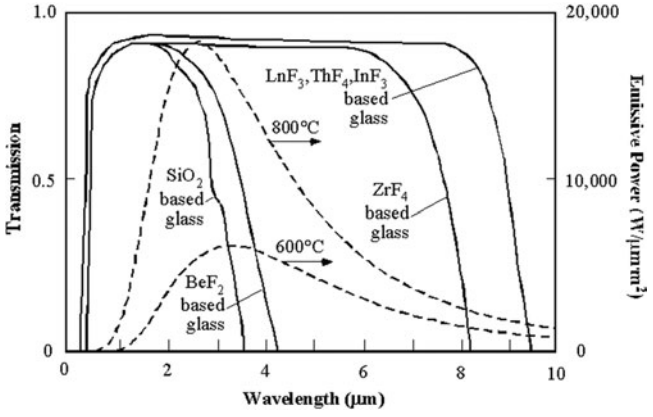

Fig. 2. Transmission through a 4-mm-thick sample of different glasses as a function of wave length,[15] compared with the emissive power of blackbody surfaces at 600 and 800°C.

because the fluid is opaque. To the left of the cutoff wavelength, the salt is transparent, and radiation heat transfer then occurs between surfaces. Near the cutoff wavelength, absorption in and emission from the salt will augment heat transfer between surfaces and the salt. For the BeF_2 glass shown in Fig. 2, absorption for typical channel hydraulic diameters of multiple millimeters will occur in the wavelength range from ~3 to 4 μm.

The actual contribution to the total heat transfer from radiation absorption, compared to convective heat transfer, will depend upon the specific conditions in the system. The potential maximum contribution of radiation heat transfer can be estimated. As specific examples, one can consider two systems, one with turbulent heat transfer that is characteristic of AHTR-MI [AHTR with metallic internals] flow channels and another with laminar heat transfer, which is similar to the conditions encountered in an NGNP intermediate heat exchanger.

In this first example, one considers turbulent heat transfer to flibe, a BeF_2-based salt, in a 2-cm-diam tube, with Reynolds number equal to 10^4, Pr = 13.5, k = 1.0 W/m K, and a surface emissivity of 1.0 (a black surface). If the tube wall temperature T_w is 700°C, and the bulk temperature of the salt T_f is 690°C, then using the Dittus Boelter relationship, the Nusselt number is 103, the convective heat transfer coefficient is 5.15 kW/m^2 K, and the convective heat flux is 51.5 kW/m^2.

For this example, based on Fig. 2, if all radiation emitted from the wall with wavelengths between λ = 2.5 μm [$(\lambda T)_{\min}$ = 2432.8 μm K] and 4.0 μm [$(\lambda T)_{\max}$ = 3892 μm K] is absorbed in the bulk of the salt (an overestimate), then the net radiative heat transfer from the wall to the salt would be

$$\dot{q}'' = \sigma \Delta F (T_w^4 - T_f^4) \ , \qquad (1)$$

where σ is the Stephan-Boltzmann constant and ΔF = 0.31 is the fraction of blackbody radiation[16] emitted between $(\lambda T)_{\min}$ and $(\lambda T)_{\max}$. For this example, $\dot{q}''$ = 0.64 kW, <2% of the convective heat flux, and thermal radiation can be neglected.

In the case of an NGNP intermediate heat exchanger, the liquid salt channels are millimeters wide, and the flow is laminar. This case can be simplified to be a 1-mm circular tube with a constant surface temperature and fully developed laminar flow; the Nusselt number is then 3.66. The convective heat transfer coefficient is 0.178 kW/m^2 K, and the heat flux is 1.78 kW/m^2. With the same assumptions as for the above example, the net radiative heat flux absorbed in the fluid is $\dot{q}''$ = ~0.6 kW/m^2, which represents 40% of the convective heat flux. Under those conditions or under the static conditions commonly used for thermal conductivity measurements, convective heat transfer is reduced, and thermal radiation effects may play an important role. Because the absorptivity of the liquid salts is not well characterized, the precise effect of thermal radiation cannot be quantified.

The above examples show that within the limit of the assumptions used, radiation heat transfer can be neglected for turbulent flows but not for laminar flow. However, each specific situation should be evaluated to determine whether thermal radiation may be important. Further work is clearly needed in the study of radiative heat transfer in liquid salt systems.

IV. SCALING LAWS

If one has the good fortune to identify a simulant fluid with suitable properties, it is possible to match prototypical values of dimensionless groups for convective heat transfer in a scaled experiment operating with reduced power and length scales. For single-phase incompressible liquids, there are four degrees of freedom to design a geometrically scaled experiment: the average operating temperature, velocity, length, and temperature difference scales. Because pressure also has an effect on gas physical properties, for gases pressure provides a fifth degree of freedom to the design of a geometrically scaled experiment.

IV.A. Selecting Scaling Parameters for Liquid Salts

Pressure has a negligible effect on liquid properties for applications of interest to nuclear reactors. However, for liquids the viscosity, density, and thermal conductivity decrease with increasing temperature. The specific heat can normally be considered constant over a wide range of temperature. The Prandtl number Pr, which is solely dependent on the fluid properties, is temperature dependent. Pr dictates the selection of the simulant liquid and its operating temperature for scaled thermofluid experiments where heat transfer phenomena are important.

For forced convection the Reynolds number Re, represents the balance between inertial and viscous forces, and thus, matching Re allows geometrically scaled experiments to reproduce flow transitions from laminar to turbulent and wall shear stresses. This imposes a condition relating the length and velocity scales for the scaled model (m) and the prototypical system (p):

$$\mathrm{Re}_m = \mathrm{Re}_p \Leftrightarrow \frac{U_m L_m}{U_p L_p} = \frac{\nu_m}{\nu_p} = \frac{\mu_m \rho_p}{\mu_p \rho_m} \ . \qquad (2)$$

If Pr is also matched, the Nusselt number for forced-convection heat transfer is also matched.

Because liquid salts have a very high boiling temperature (>1300°C) and a very low volatility, phase change phenomena are typically not important. However, in cases where free surfaces exist between the liquid and a gas, as at the free surface of liquid pools or centrifugal pump bowls, or in cases where gas bubbles are entrained or liquid jets or droplets are sprayed through a gas, gravity forces may play an important role. In these

cases the Froude number should also be matched, which imposes another condition relating the length and velocity scales:

$$\mathrm{Fr}_m = \mathrm{Fr}_p \Rightarrow \frac{U_m}{U_p} = \left(\frac{L_m}{L_p}\right)^{1/2} \quad . \tag{3}$$

In the case where the Reynolds and Froude numbers are matched simultaneously, Eqs. (2) and (3) then specify the model length scale value as a function of properties of the prototypical and model fluids:

$$\left.\begin{aligned}\mathrm{Re}_m &= \mathrm{Re}_p \\ \mathrm{Fr}_m &= \mathrm{Fr}_p\end{aligned}\right\} \Leftrightarrow \left(\frac{L_m}{L_p}\right)^{3/2} = \frac{\nu_m}{\nu_p} = \frac{\mu_m \rho_p}{\mu_p \rho_m} \quad . \tag{4}$$

Transient hydrodynamic phenomena, such as oscillating flow forcing functions, are preserved by matching the Strouhal number:

$$\mathrm{Sr}_m = \mathrm{Sr}_p \Leftrightarrow \frac{\tau_m}{\tau_p} = \frac{L_m}{U_m}\frac{U_p}{L_p} = \frac{\tau_{conv,m}}{\tau_{conv,p}} \quad , \tag{5}$$

where τ is the timescale for the transient phenomena and the convective timescale is defined as $\tau_{conv} = L/U$. The relative acceleration of transient phenomena in the scaled experiment is then given by the ratio of fluid transit times L/U.

For the case of buoyancy-driven flows, the scaling procedure is identical except that now the velocity scale is defined with the buoyant velocity scale, $U_b \equiv (gL\beta\Delta T)^{1/2}$. The Grashof number must then be matched in place of the Reynolds number. The Prandtl number must also be matched to obtain similitude. It is convenient to algebraically decompose the Grashof number into two dimensionless groups[16]: gL^3/ν^2 and $\beta\Delta T$. In the last group, ΔT is the system temperature difference scale, typically taken to be the difference between the maximum and minimum fluid temperatures in the system. To simulate natural or mixed convection, the $\beta\Delta T$ dimensionless group imposes

$$(\beta\Delta T)_m = (\beta\Delta T)_p \Rightarrow \frac{\beta_m}{\beta_p} = \frac{\Delta T_p}{\Delta T_m} \quad ; \tag{6}$$

thus, the temperature difference–scale ratio is fixed by the thermal expansion coefficient ratio. The other group imposes

$$\left(\frac{gL^3}{\nu^2}\right)_m = \left(\frac{gL^3}{\nu^2}\right)_p \Rightarrow \left(\frac{L_m}{L_p}\right)^{3/2} = \frac{\nu_m}{\nu_p} \quad , \tag{7}$$

which is identical to the length scale requirement to simultaneously match Re and Fr, Eq. (4). Thus, experiments scaled to reproduce Fr can also reproduce Gr if an appropriate value for ΔT is selected using Eq. (6). If transients are investigated, the Strouhal number should also be matched as for forced convection, and the scaling is identical except that the velocity scale is defined based on the buoyant velocity scale U_b.

In high-temperature heat transfer where large temperature changes may occur, the variation of fluid properties with temperature, particularly the variation of viscosity, may be important. Matching this variation imposes other restrictions on the temperature difference scale that can be compared with Eq. (6) to estimate the degree of distortion in the scaled experiment.

As stated earlier, matching the governing differential equations is not sufficient to reproduce fluid mechanics and heat transfer; the boundary and initial conditions also must be properly scaled. For fluid mechanics, this requires the use of geometric scaling of the fluid boundaries created by pipe and vessel walls and inlets and outlets. For heat transfer this scaling also determines the optimal thermal properties of container materials in the scaled facility. For steady-state heat flux similitude, the modified Biot number must be matched. For heat transfer through thin structures ($l \ll L$), such as heat exchanger tubes, the option exists to adjust the scaled structure thickness using a different scaling ratio than that for the other system dimensions:

$$\mathrm{Bi}_m^* = \mathrm{Bi}_p^* \Rightarrow \frac{\lambda_m}{\lambda_p} = \frac{k_m}{k_p} \cdot \frac{l_m L_p}{l_p L_m} \quad . \tag{8}$$

To accurately scale the heat flux through an interface, the ratio of the solid thermal conductivity λ must be similar to the ratio of the liquid thermal conductivity k multiplied by the ratios of length scales. This condition suffices to replicate steady-state heat transfer between fluids and structures, while for transients, the transient thermal response of the container must be reproduced as well. Scaling of the transient conduction equation for the solid material gives the Fourier number, which must also be matched:

$$\mathrm{Fo}_m = \mathrm{Fo}_p \Rightarrow \frac{\alpha_m}{\alpha_p} = \frac{l_m^2 \tau_p}{l_p^2 \tau_m} \quad , \tag{9}$$

placing a constraint on the model container thermal diffusivity α_m.

Because the timescales τ are determined in scaling the fluid mechanics, matching the Strouhal number introduces the convective timescales in Eq. (9):

$$\mathrm{Fo}_m = \mathrm{Fo}_p \Rightarrow \frac{\alpha_m}{\alpha_p} = \frac{l_m^2 L_p U_m}{l_p^2 L_m U_p} \quad . \tag{10}$$

Because the length and velocity scales have already been defined, Eq. (10) determines the optimal thermal diffusivity for the scaled container material.

Finally, one must check that the scaled container material is chemically and mechanically compatible with

the simulant fluid when used at the desired experimental temperatures. Because of the potential for pressurizing the experiment if helium is simulated, stress analysis of the container material may be required. If it is not possible to obtain a desirable material for the scaled container, one can perform iterations by selecting another fluid, or accept some distortion in the experiment phenomenology.

When surface tension–dominated free surface effects, gas entrainment, or droplet generation are important, the condition on the Weber number imposes

$$\mathrm{We}_m = \mathrm{We}_p \Leftrightarrow \frac{U_m^2 L_m}{U_p^2 L_p} = \frac{\sigma_m \rho_p}{\sigma_p \rho_m} \quad . \tag{11}$$

Combined with matching the Froude number [Eq. (3)], free surface, gas entrainment, and droplet generation effects resulting from the balance of inertia, gravity, and surface tension forces can be simulated.

IV.B. Selecting Scaling Parameters for Helium

To model helium in the environment typically envisioned for nuclear reactors and other high-temperature heat transport applications (5 to 10 MPa; 600 to 1000°C), the use of ideal gas approximation to estimate the density variation with temperature and pressure is accurate. One has

$$\rho(T,P) = \rho_0(T_0,P_0)\cdot\frac{P}{P_0}\cdot\frac{T_0}{T} \quad , \tag{12}$$

where T_0 and P_0 are reference absolute temperature and pressure, respectively, and ρ_0 is the gas density at T_0 and P_0.

The theory of viscosity developed by Maxwell[17] can be used for understanding gas scaling, which is useful in the early stages of an experiment design. However, later, when designing a final experiment, accurate data must be used instead of this simplified model.

The dynamic viscosity of a pure gas is independent of pressure and varies with temperature approximately as

$$\mu(T) = \mu_0(T_0)\cdot\left(\frac{T}{T_0}\right)^{1/2} \quad . \tag{13}$$

Equation (13) shows that the viscosity increases with the square root of the temperature, while experiments suggest a power from 0.6 to 1.0. Similarly, the thermal conductivity can be approximated as

$$k(T) = k_0(T_0)\cdot\left(\frac{T}{T_0}\right)^{1/2} \quad . \tag{14}$$

As with the procedure presented for liquids, the need to match the Prandtl number for heat transfer preselects candidate simulant fluids. However, this selection is easier for gases than for liquids because monoatomic and diatomic gases have similar Prandtl numbers, which are only weakly dependent on temperature and pressure.

To match the Reynolds number, and simulate forced convection, Eq. (2) must be satisfied. However, for experiments where liquid free surfaces are also present, the liquid Froude number is also relevant and should be matched. In this situation, where an integral experiment simulating both liquid salt and helium phenomena is desired, the equation for scaling is then Eq. (4). One can substitute into Eq. (4) the values of ρ and μ from Eqs. (12) and (13). Choosing the same reference temperatures and pressures for the model and prototype systems, one obtains, after rearranging the terms,

$$\mathrm{Re}_m = \mathrm{Re}_p \Rightarrow \frac{P_m}{P_p} = \frac{\rho_{0,p}\,\mu_{0,m}}{\rho_{0,m}\,\mu_{0,p}}\left(\frac{T_m}{T_p}\right)^{3/2}\left(\frac{L_p}{L_m}\right)^{3/2}$$

$$= \frac{\nu_{0,m}}{\nu_{0,p}}\left(\frac{T_m}{T_p}\right)^{3/2}\left(\frac{L_p}{L_m}\right)^{3/2} \quad . \tag{15}$$

Note that here the length and temperature are coupled such that the average absolute temperature of the model fluid T_m decreases with the same proportion as its length scale L_m. For example, a gas at 300 K (room temperature) simulates the same gas at 1000 K when used in a 30% length scale facility. If the simulant gas is well chosen, to have a smaller reference kinematic viscosity than the prototype gas, its total pressure can also be significantly reduced compared to the prototype while still matching the Reynolds number. As mentioned earlier, experiments suggest that the viscosity increases with temperature to the 0.6 to 1.0 power; then, for a scaling behavior analogous to Eq. (15) to still be applicable, one simply needs to scale velocity with length to the same power. This results in an even more favorable velocity scaling.

For forced convection the container material properties can be chosen using the same procedure presented for liquids. The model length scale can be adjusted to find a desirable match for the container thermal properties.

In buoyancy-driven flows, the Prandtl and Grashof numbers must be matched. For an ideal gas, the thermal expansion coefficient is simply the inverse of temperature. Hence, matching the first dimensionless group constituting the Grashof number, Eq. (6) reduces to

$$(\beta\Delta T)_m = (\beta\Delta T)_p \Leftrightarrow \frac{\Delta T_m}{\Delta T_p} = \frac{T_m}{T_p} \quad . \tag{16}$$

Here, the temperature difference scale decreases linearly with the model average absolute temperature. Matching the second dimensionless group gL^3/ν^2 is equivalent to matching the Reynolds number as is done for forced convection, and the same scaling laws as for Eq. (15) apply, i.e., $\Delta T_m/\Delta T_p = T_m/T_p = L_m/L_p$. Therefore, for gas natural or mixed convection simulation, the length

scale decreases linearly with the temperature difference scale and the average absolute temperature.

The condition deriving from Eq. (16) also allows the variation of gas properties with temperature to be matched, including viscosity. For a gas based on Eq. (12), we have $\gamma = -1/2T$, and based on Eq. (14), $\kappa = -1/2T$. This implies that for an ideal gas, the viscosity and thermal conductivity linear variations are accurately reproduced for forced and natural convection when the conditions of Eqs. (15) and (16) are respected.

V. SELECTION OF POTENTIAL SIMULANT-FLUID CANDIDATES

The selection of optimal scaling parameters for several categories of liquid fluoride salts—beryllium, zirconium, sodium fluoroborate, and alkali-based salts (Table I)—is studied here. The thermophysical properties of these liquid salts have been characterized in the past but not at very high temperatures (>750°C). Also, while the thermal conductivity of flibe has been measured accurately, the measurement of thermal conductivity at high temperatures with transparent fluids is challenging, and significantly greater uncertainty exists for the other salts. Thus, while the scaling parameters have been calculated using the best available thermophysical property estimates for these salts, the scaling may change as better properties become available.

To simulate liquid fluoride salts in geometrically scaled experiments, three classes of simulant fluids have been identified. Table II reviews their properties. The first fluid category is low-viscosity heat transfer fluids, such as Solutia Therminol® VP-1. Therminol® VP-1 is a synthetic organic fluid, commercialized by several chemical companies under different names, such as Dowtherm A (from Dow Chemical) or Xceltherm MK1 (from Radco Industries). It is a eutectic mixture containing 73.5% diphenyl oxide and 26.5% biphenyl by weight. This fluid has a low flammability, with a flash point of 124°C and an autoignition temperature of 612°C. Its boiling temperature is 257°C, and it is recommended for use to temperatures up to 400°C. Therminol® VP-1 is not optically clear, which forbids optical investigation methods.

Light mineral oils such as Drakesol® 260-AT, manufactured by Penreco, constitute the second class of liquid salt simulants. Drakesol® 260-AT is inexpensive, odorless, colorless, stable, nontoxic, food-grade mineral oil. It has a high index of refraction, $n = 1.4498$ at 40°C, which nearly matches that of fused silica (1.4575) and of Pyrex (1.47), allowing the use of optical investigation techniques such as particle image velocimetry for flow field characterization and laser-induced fluorescence for temperature measurements. The high refractive index of this light mineral oil and its low viscosity make it an unusual fluid and render it attractive to conduct fluid dynamics as well as heat transfer experiments at moderate temperature. Even though it has a high boiling temperature, 268°C, the oil was noticed to degrade when used at temperatures >120°C. Therefore, employing this oil at such temperatures requires a constant monitoring of the viscosity. The Drakesol oil has moderate flammability with a flash point of 127°C and an autoignition temperature of 220°C. Drakesol is similar to the oil used in the Matched Index of Refraction Facility at Idaho National Laboratory.[18]

Finally, for experiments where only the fluid mechanics are of interest, water can provide an outstanding simulant fluid for liquid salts. While it is possible to match liquid salt Prandtl numbers with water, its viscosity changes too rapidly to accurately reproduce heat transfer phenomena. The scaling for Re and Fr for water and for the oils is very similar. For fluid mechanics experiments water has the practical advantage of evaporating if it is spilled, making it easier to work with. For this reason, water may also be used for leak and

TABLE II

Liquid Salt Potential Simulants

	T (°C)	ρ (kg/m^3)	ν (m^2/s $\times 10^6$)	σ (N/m $\times 10^3$)	C_P (kJ/kg·K)	k (W/m·K)	Pr
Therminol® VP-1[a]	38	1050	2.73	38	1.60	0.135	34.1
	104	995	0.93	31	1.79	0.127	13.1
	204	909	0.38	20	2.06	0.113	6.3
Drakesol® 260-AT	40	795[b]	3.8[b]	25[b]	2.00 (Ref. 18)	~0.098 (Ref. 18)	65.0
	80	775[b]	1.9[b]	22[b]	2.00 (Ref. 18)	~0.098 (Ref. 18)	30.8
Water	22	1002 (Ref. 16)	0.96 (Ref. 16)				

[a]Given by the manufacturer.
[b]Measurements made by the authors. Water can be used to simulate liquid salt hydrodynamics.

proof testing of heat transfer flow loops before they are filled with oil.

In Sec. IV, the scaling laws for helium were presented. It was concluded that to reproduce helium fluid mechanics in geometrically scaled experiments at a reduced length scale, a gas with a lower kinematic viscosity was necessary. Nitrogen and air are good candidates for working fluids for scaled experiments to reproduce high-temperature, high-pressure helium phenomena. Nitrogen may be preferable because it is a pure inert gas. The properties of high-pressure and high-temperature helium are presented along with nitrogen properties in Table III.

For liquid fluoride salts, high-nickel alloys and carbon-based materials are commonly used materials for construction. Here, Haynes 214, 316 stainless steel; Incoloy® 800H; and Hastelloy N are selected as representative of potential metallic container materials, and graphite is representative for carbon-based materials. Their thermal properties at high temperature are summarized in Table IV, as well as properties of a nonexhaustive list of candidate model materials. It is commonly desirable to build models in glass, which aids flow visualization. Thus, fused silica and Pyrex are considered here. Also, certain high-thermal-conductivity epoxies and thermoplastics may offer improved scaling of the prototype materials, particularly graphite. Furthermore, the thermal conductivity and diffusivity of such epoxies and thermoplastics can be adjusted by changing their additives and processing methods, and they can be cast and machined into complex shapes, for example to simulate graphite blanket blocks and fuel elements. Titanium is also an attractive candidate for simulating high-temperature alloys.

TABLE III

Helium and Nitrogen Thermophysical Properties

	Temperature and Pressure	ρ (kg/m^3)	μ (kg/m·s $\times 10^6$)	ν (m^2/s $\times 10^6$)	C_P (kJ/kg·K)	k (W/m·K)	Pr
Helium	0.1 MPa; 300 K (Ref. 20)	0.16	19.9	124.2	5.20	0.154	0.70
	10 MPa; 1000 K (Ref. 20)	4.7	51.8	13.3	5.20	0.36	0.66
Nitrogen	0.1 MPa; 300 K (Ref. 21)	1.14	17.8	15.6	1.04	0.026	0.71
	1.1 MPa; 400 K (Ref. 21)	9.3	22.5	1.4	1.05	0.032	0.69

TABLE IV

Thermal Properties of Candidate Materials of Construction for the Prototype and for the Model

	T (°C)	ρ (kg/m^3)	C_P (kJ/kg·K)	k (W/m·K)	α (m^2/s $\times 10^6$)	T_{max}[a] (°C)
Prototype						
Haynes® 214[b]	700	8000	0.67	26.9	5.0	1300
Stainless steel 316 (Ref. 16)	700	8200	0.43	24.2	6.9	850
Hastelloy® N[b]	700	8800	0.58	23.6	4.6	982
Incoloy® 800H[b]	700	7900	0.46	22.8	6.3	1100
Graphite H-451[c]	700	1700	1.90	32.4	9.9	3000
Model						
Fused silica[d]	25	2200	0.90	1.6	0.81	1000
Pyrex 7740[d]	25	2230	1.18	1.4	0.53	290
Thermally conductive epoxy[d]	25	1800		2.5		350
Thermally conductive polyphenylene sulfide[d]	25	2200	1.0	3.5	2.3	350

[a]T_{max} indicates the maximum operating temperature.
[b]Given by the manufacturer.
[c]Idaho National Engineering and Environmental Laboratory/General Atomics values.
[d]Typical values.

VI. SELECTION OF SCALING PARAMETER VALUES

Careful selection of length, velocity, pressure, and temperature scales for experiments can allow the coupling between important thermal and hydraulic phenomena to be reproduced. All scaled experiments involve some distortion of phenomena, so appropriate scaling requires the identification of the most important phenomena that govern the integral system response and appropriate selection of the available adjustable parameter values to reproduce the important phenomena at reduced geometric scale, recognizing that other phenomena may suffer distortion. Methods for scaling for integral experiments have been extensively developed for light water reactor (LWR) accident studies, where it is too expensive to perform integral test experiments at full scale and power, so reduced-scale facilities are studied instead to provide the basis for licensing.[19] Because of a lack of appropriate simulant fluids, these LWR test facilities have used water as the simulant fluid and typically must be scaled with a relatively large reduction in flow area, with associated distortion, to achieve acceptable power input. Also, commonly these experiments simulate only decay power levels. Similar design methods can be applied to high-temperature systems using liquid salts and high-pressure helium as heat transport fluids. But, the availability of low-temperature simulant fluids that can replicate convective heat transfer phenomena at reduced length and greatly reduced power scales provides a significant advantage for liquid salt and high-pressure helium integral effects test facilities, for systems where thermal radiation heat transfer is small compared to convective heat transfer.

For the simulant fluids discussed here, reduced height, geometrically scaled experiments are used to preserve Fr at reduced length and power scales. Because the flow path length drops faster than the velocity, a reduced geometric scale requires time acceleration. Three primary approaches are available for scaling the cross-sectional dimensions of scaled experiments. Geometric scaling can be used, which preserves the ratios of all geometric dimensions in the system. To further reduce the experiment power and flow rates, the flow areas can be further reduced. In modular systems, where flow occurs in multiple, similar parallel channels, the natural choice is to replicate geometrically a subset of the flow channels. The primary distortions from reducing the number of modules come from potential interactions between the parallel flow paths, such as effects that would cause nonuniform flow distribution between channels or coupling and instability effects.

Where modularity is not available or where coupling effects are expected to be important, the stream-tube approach can be used to reduce the flow path area. Here, a physical flow boundary is substituted along a surface that would have (at least time averaged) parallel flow in the prototypical systems. Distortions here come primarily from the incorrect momentum and heat fluxes introduced by the artificial solid boundaries.

Because scaled experiments inherently involve some distortions of phenomena, the designs often include the capability to vary parameters such as power, temperature, flow velocity, or geometric configuration. The response of the system to such parametric variations can often identify the relative roles of different phenomena and increase the confidence in the capability of models to predict the integral system performance.

The primary goals of scaling of experiments are to reproduce dominant system phenomena with low distortion, in experiments performed at reduced power, length, temperature, and power scales. The mechanical pumping power can be estimated as

$$Qp = \Delta P \cdot Q = \rho U^3 L^2 \quad , \tag{17}$$

where ΔP is the pressure drop across the system and Q is the volumetric flow rate. The heating power is

$$Qh = \rho C_P \Delta T \cdot Q = \rho C_p \Delta T U L^2 \quad . \tag{18}$$

The simulants introduced above can be used to simulate helium and liquid salt incompressible momentum and convective heat transfers at reactor operational and accidental conditions when no phase changes are involved and when thermal radiation is unimportant or can be corrected for. Fluids are considered incompressible when the Mach number, $M = u/c$, is <0.3, where u is the fluid velocity and c is the fluid speed of sound. For ideal gases (as helium and N_2 in the conditions considered here), the speed of sound is $c = \sqrt{\gamma RT/m}$, where γ is the heat capacity ratio, R is the ideal gas constant, T is the temperature in kelvin, and m is the molar mass. Flibe's speed of sound is ~3300 m/s at 650°C, and the Penreco and Therminol oil sound speeds are on the order of 1500 m/s at room temperature.

The scaling laws introduced previously to select scaling parameters for geometrically scaled experiments are now applied to illustrate typical pumping and heating power scaling. The temperature of the model liquid is selected to match the Prandtl number. With the exception of NaF-$NaBF_4$, Therminol® VP-1 can simultaneously reproduce the Reynolds, Froude, Prandtl, and Grashof numbers for the key liquid salts studied here. Table V shows that flibe and flinak are simulated with scales reduced to ~40% for the length, 63% for the velocity, and ~30 to 40% for the temperature difference. The bold italic entries in Table V, for the oil temperature, length scale, velocity scale, and ΔT scale, provide four adjustable parameters. Because it is desired to match Pr, Re, Fr, and Gr, the oil temperature is set to match Pr, and the three remaining parameters are set to simultaneously satisfy Eq. (2) (for Re), Eq. (3) (for Fr), and Eq. (6) (for Gr). The scaled system accelerates time to ~63% of the prototypical times. Because the NaF-ZrF_4 thermal conductivity is

TABLE V

Liquid Salts Simulated by Therminol® VP-1

	Flibe (600°C)	Flibe (900°C)	NaF-ZrF_4 (700°C)	NaF-$NaBF_4$ (700°C)	Flinak (700°C)
Heat transfer fluid temperature	80°C	215°C	110°C	>400°C	230°C
***Length scale*, L_m/L_p**	0.44	0.38	0.64	—	0.38
***Velocity scale*, U_m/U_p**	0.66	0.62	0.80	—	0.62
ΔT *scale*, $\Delta T_m/\Delta T_p$	0.29	0.29	0.35	—	0.38
Reynolds number, Re_m/Re_p	1	1	1	—	1
Froude number, Fr_m/Fr_p	1	1	1	—	1
Weber number, We_m/We_p	0.57	0.59	No data	—	No data
Prandtl number, Pr_m/Pr_p	1	1	1	—	1
$\beta\Delta T$, $\beta_m \Delta T_m/\beta_p \Delta T_p$	1.02	1	1	—	1
$\gamma\Delta T$, $\gamma_m \Delta T_m/\gamma_p \Delta T_p$	0.56	0.63	0.91	—	0.43
$\kappa\Delta T$, $\kappa_m \Delta T_m/\kappa_p \Delta T_p$	No data	No data	No data	—	No data
Grashof number, Gr_m/Gr_p	1	1	1	—	1
Pumping power, Qp_m/Qp_p	0.029	0.017	0.066	—	0.015
Heating power, Qh_m/Qh_p	0.014	0.011	0.056	—	0.017

smaller than the other salts, it requires a larger model length scale.

Table V shows that the scaled systems require only a small fraction of the prototype pumping and heating power, typically <2%, which can be economically attractive particularly when simulating protracted transients. Because the temperature difference scale ratio is similar to the length scale ratio, one can conclude according to the argument in Sec. IV.A that thermal expansion phenomena such as pool level swell are accurately reproduced by this similitude. However, the variation of viscosity with temperature is not reproduced as accurately, varying by a ratio from 0.43 to 0.91. This can have effects on phenomena controlled by viscosity changes, such as in the salt flow distribution in compact plate heat exchangers operating with large salt temperature changes, as occurs in the NGNP intermediate heat exchanger.

The oil scaling sets the desired thermal properties of the container material. For Eq. (8) for heat transfer similitude to be respected, in the case where the solid and fluid length scale ratio is conserved, the model container material thermal conductivity must be $\lambda_m/\lambda_p = k_m/k_p = 0.091$, when the salt is flibe. If the solid thermal conductivity of the model container λ_m is too small, the dimensionless heat transfer through the model wall is also too small. This can be corrected by using a scaled container with thinner walls, thus adjusting the ratio l_m/l_p in Eq. (8). Adjusting the wall thickness can be expected to have small effects when the wall is thin compared to other system dimensions, $\boldsymbol{L} \gg l$. For transient response, the requirement for Fourier number similarity, Eq. (10), imposes the container thermal diffusivity: $\alpha_m/\alpha_p = 0.25$. If this ratio is too small, the model solid structures have a slower response time to transients than the liquid, and their action as heat source or sink is reduced. Again, the model solid structures can be made thinner to compensate for this effect, thus adjusting the ratio l_m/l_p in Eq. (10).

Thermally conductive epoxies and plastics provide the best similitude because their properties can be adjusted upon request to the manufacturer. In contrast to fused silica and Pyrex, they are not transparent.

If the model uses light mineral oils like Drakesol® 260-AT, flibe and NaF-ZrF_4 can be simulated, but the properties of the oil must be continuously monitored. However, the temperatures required to simulate NaF-$NaBF_4$ and flinak are too high to be practical with this oil. The scaling for flibe and NaF-ZrF_4 is also possible with the heat transfer fluid presented in Table VI. However, the temperature difference scale is slightly increased, the viscosity variations are too important, and the input powers to the mineral oils are smaller than for heat transfer fluids. This is balanced by the chemical stability of heat transfer oils, which prevents their viscosity from varying with time when exposed to high temperatures, and the well-understood and documented thermophysical property data for the heat transfer oils.

For convection, the scaling of helium by nitrogen leads to results like those presented in Table VII. If one follows the scaling presented in Sec. IV.B, 10 MPa and 727°C (1000 K), helium is optimally simulated with 127°C (400 K) N_2 at a reduced length scale of 40%, velocity scale of 63%, and ΔT scale of 39%. In this case the pressure scale is 11%, allowing the model to use nitrogen at a significant reduced pressure of 1.1 MPa. These length, velocity, and ΔT scales are similar to those found for scaled liquid salt experiments, as can be seen by comparing Table V with the first column of Table VII. Any coupled experiment that simulates heat transfer between

TABLE VI

Liquid Salts Simulated by Drakesol® 260AT

	Flibe (600°C)	Flibe (700°C)	$NaF\text{-}ZrF_4$ (700°C)	$NaF\text{-}NaBF_4$ (700°C)	Flinak (700°C)
Mineral oil temperature	110°C	135°C	130°C	>150°C	>150°C
***Length scale*, L_m/L_p**	0.40	0.39	0.59	—	—
***Velocity scale*, U_m/U_p**	0.63	0.62	0.77	—	—
ΔT *scale*, $\Delta T_m/\Delta T_p$	0.36	0.36	0.44	—	—
Reynolds number, Re_m/Re_p	1	1	1	—	—
Froude number, Fr_m/Fr_p	1	1	1	—	—
Weber number, We_m/We_p	0.62	0.66	No data	—	—
Prandtl number, Pr_m/Pr_p	1	1	1	—	—
$\beta\Delta T$, $\beta_m\Delta T_m/\beta_p\Delta T_p$	1	1	1	—	—
$\gamma\Delta T$, $\gamma_m\Delta T_m/\gamma_p\Delta T_p$	1.44	1.80	1.86	—	—
$\kappa\Delta T$, $\kappa_m\Delta T_m/\kappa_p\Delta T_p$	No data	No data	No data	—	—
Grashof number, Gr_m/Gr_p	1	1	1	—	—
Pumping power, Qp_m/Qp_p	0.015	0.014	0.038	—	—
Heating power, Qh_m/Qh_p	0.012	0.011	0.048	—	—

TABLE VII

Helium Scaling by Nitrogen for Cases Consistent with Liquid Salt Scaling (Table V)

	Helium (1000 K; 10 MPa)		
N_2 temperature	400 K	400 K	300 K
***Pressure scale*, P_m/P_p**	0.11	0.05	0.05
***Length scale*, L_m/L_p**	0.40	0.67	0.49
***Velocity scale*, U_m/U_p**	0.63	0.82	0.70
ΔT *scale*, $\Delta T_m/\Delta T_p$	0.39	0.39	0.29
Reynolds number, Re_m/Re_p	1	1	1
Froude number, Fr_m/Fr_p	1	1	1
Prandtl number, Pr_m/Pr_p	1	1	1
$\beta\Delta T$, $\beta_m\Delta T_m/\beta_p\Delta T_p$	1	1	1
$\gamma\Delta T$, $\gamma_m\Delta T_m/\gamma_p\Delta T_p$	1	1	1
$\kappa\Delta T$, $\kappa_m\Delta T_m/\kappa_p\Delta T_p$	1	1	1
Grashof number, Gr_m/Gr_p	1	1	1
Pumping power, Qp_m/Qp_p	0.080	0.22	0.098
Heating power, Qh_m/Qh_p	0.016	0.026	0.012

liquid salt and helium must use the same length and temperature difference scales for both fluids. Because the differences between the gas and liquid scales are relatively small, experiments with both liquid salts and helium can be designed with relatively small distortion.

As explained in Sec. V, the gas property variations are reproduced accurately with this scaling. To allow operation at lower pressures, scaling alternatives were examined to reduce the pressure to 5% of the prototypical value. This scaling does not preserve the liquid Fr for coupled experiments with salts and helium but can preserve Re. According to Eq. (15) lower-pressure operation can be achieved by increasing the length scale or reducing the model temperature. Table VII presents both alternatives. First, N_2 is kept at a temperature of 127°C (400 K), and hence, the length scale is changed. This configuration requires larger length and velocity scales, and the pumping and the heating powers become much larger. Next, the temperature is reduced to 27°C (300 K), so the length scale is 50% of the prototype. This

alternative can be viable because the pumping and the heating powers are of the same order or smaller than for the 127°C (400 K), 11% pressure scale case, but the effects of helium property variations are now overestimated by a factor $(L_m/L_p)/(\Delta T_m/\Delta T_p) = 1.7$. Clearly, room-temperature heat transfer and fluid mechanics experiments with nitrogen (or air) can provide data with direct relevance to high-temperature, high-pressure processes with helium.

The simulation of heat transfer to container materials for the gases is similar to that of the liquids. The ratios of the nitrogen and helium thermal conductivities as well as the thermal diffusivities are the same order as the ratios for the liquids. Thus, the comments made previously for the liquid scaling also applies to the gases.

VII. CONCLUSIONS

Two new categories of liquids, gases, and structural materials have been presented that allow the simulation of transient fluid mechanics and high-temperature convective heat transfer phenomena in systems with liquid salts, high-pressure helium, and their structures in scaled facilities with relatively small distortion. These methods can be applied to the simulation of systems where radiative heat transfer is not a dominant phenomena.

Heat transfer oils are particularly promising because of their excellent thermal properties, which permit scaled fluid mechanics and heat transfer experiments at substantially reduced length, velocity, temperature, and power scales. When used with fused silica or Pyrex, these fluids can simulate liquid salts and their surrounding metallic structures with an uncommonly small distortion. This permits the design of scaled integral liquid salt experiments with low distortion of key fluid mechanics and convective heat transfer phenomena. Liquid salt thermal properties also need to be better characterized at high temperatures, particularly the thermal conductivity and surface tension for salts other than flibe.

Dimensional analysis for helium, which can be considered as an ideal gas in the temperature and pressure range of interest, leads to the selection of nitrogen (another ideal gas) to simulate helium in a scaled facility. Simplified gas property relationships lead to simple scaling laws for ideal gases. Those laws, when applied, also guarantee that the gas-scaled thermal variations are accurately reproduced, allowing one to conduct scaled integral experiments of high-temperature and high-pressure helium fluid mechanics and heat transfer phenomena with low-temperature and medium-pressure nitrogen or air. Sound speeds do not scale, so these experiments must be limited to cases where helium compressibility effects are small.

Finally, it is remarkable that the container heat transfer scaling rules for the helium-nitrogen scaling are the same as for the heat transfer fluid–liquid salt scaling and thus permit the design of coupled experiments that can reproduce high-temperature convective heat transfer phenomena with both liquid salt and helium simultaneously.

NOMENCLATURE

C_p = isobaric specific heat

g = acceleration of gravity

k = fluid thermal conductivity

L = fluid characteristic length scale

l = solid characteristic length scale

P = pressure

Q = volumetric flow rate

Qh = heating power, $Qh = \rho C_P \Delta T \cdot Q$

Qp = mechanical pumping power, $Qp = \Delta P \cdot Q$

T = temperature

U = velocity scale

U_b = buoyant velocity scale, $U_b \equiv (gL\beta\Delta T)^{1/2}$

Greek

α = thermal diffusivity

β = coefficient of thermal expansion, $\beta = -(1/\rho)(\partial\rho/\partial T)|_{T_0, P_0}$

γ = coefficient of viscosity linear thermal change, $\gamma = -(1/\mu)(\partial\mu/\partial T)|_{T_0, P_0}$

ΔP = pressure drop across the system

ΔT = temperature difference scale

κ = coefficient of thermal conductivity linear thermal change, $\kappa = -(1/k)(\partial k/\partial T)|_{T_0, P_0}$

λ = solid thermal conductivity

μ = dynamic viscosity

ν = kinematic viscosity

ρ = density

τ = timescale

σ = surface tension

Dimensionless Groups

Bi* = modified Biot number, $\text{Bi}^* \equiv k \cdot l/\lambda \cdot L$

Fo = Fourier number, $\text{Fo} \equiv l^2/\alpha\tau$

Fr = Froude number, Fr $\equiv U^2/gL$

Gr = Grashof number, Gr $\equiv gL^3\beta\Delta T/\nu^2$

Pr = Prandtl number, Pr $\equiv \nu/\alpha$

Re = Reynolds number, Re $\equiv UL/\nu$

St = Strouhal number, Sr $\equiv \tau U/L$

We = Weber number, We $\equiv \rho U^2 L/\sigma$

Subscript

0 = reference absolute value

conv = convection

m = model

p = prototype

ACKNOWLEDGMENTS

Technical advice on fluoride salt optical properties from David Williams at ORNL is gratefully acknowledged. Support for this work was provided by the U.S. Department of Energy under Nuclear Energy Research Initiative grant DE-FC07-05ID14669.

REFERENCES

1. "A Review of Molten-Salt Reactor Technology," *Nucl. Appl. Technol.*, **8**, *2* (1970).

2. D. F. WILLIAMS, L. M. TOTH, K. T. CLARNO, and C. W. FORSBERG, "Assessment of Properties of Candidate Liquid Salt Coolants for the Advanced High Temperature Reactor (AHTR)," ORNL/GEN4/LTR-05-001, Oak Ridge National Laboratory (2005).

3. R. W. MOIR et al., "HYLIFE-II: A Molten-Salt Inertial Fusion Energy Power Plant Design—Final Report," *Fusion Technol.*, **25**, 5 (1994).

4. P. F. PETERSON, "Design Methods for Thick-Liquid Protection of Inertial Fusion Chambers," *Fusion Technol.*, **39**, 702 (2001).

5. J. M. RYSKAMP et al., "Next Generation Nuclear Plant—High-Level Functions and Requirements," INEEL/EXT-03-01163, Idaho National Engineering and Environmental Laboratory (Sep. 2003).

6. C. W. FORSBERG, P. F. PETERSON, and P. S. PICKARD, "Molten-Salt–Cooled Advanced High Temperature Reactor for Production of Hydrogen and Electricity," *Nucl. Technol.*, **144**, 289 (2003).

7. S. J. KLINE, *Similitude and Approximation Theory*, Springer-Verlag (1986).

8. M. N. ÖZIŞIK, *Radiative Transfer and Interactions with Conduction and Convection*, John Wiley and Sons, New York (1973).

9. P. A. KOTTKE, T. P. FERGUSON, and A. G. FEDOROV, "Scale Analysis of Combined Thermal Radiation and Convective Heat Transfer," *J. Heat Transfer*, **126**, 250 (2004).

10. D. K. KIM and R. VISKANTA, "Interaction of Convection and Radiation Heat Transfer in High Pressure and Temperature Steam," *Int. J. Heat Mass Transfer*, **27**, *6*, 939 (1984).

11. J. S. CHIOU, "Combined Radiation-Convection Heat Transfer in a Pipe," *J. Thermophys. Heat Transfer*, **7**, *1*, 178 (1993).

12. R. SIEGEL and J. R. HOWELL, *Thermal Radiation Heat Transfer*, 4th ed., Chap. 11-7.5, Taylor and Francis, New York (2002).

13. J. W. COOKE, "Molten-Salt Reactor Semiannual Progress Report Period Ending August 31, 1972," ORNL-4832, p. 36, Oak Ridge National Laboratory (1972).

14. J. W. COOKE, "Development of the Variable-Gap Technique for Measuring the Thermal Conductivity of Fluoride Salt Mixtures," ORNL-4831, Oak Ridge National Laboratory (Feb. 1973).

15. J. LUCAS, "Review of Fluoride Glasses," *J. Mater. Sci.*, **24**, 1 (1989).

16. F. P. INCROPERA and D. P. DeWITT, *Fundamentals of Heat and Mass Transfer*, 4th ed., John Wiley and Sons, New York (1996).

17. R. B. BIRD, W. E. STEWART, and E. N. LIGHTFOOT, *Transport Phenomena*, John Wiley and Sons (1960).

18. C. STOOTS, S. BECKER, K. CONDIE, F. DURST, and D. McELIGOT, "A Large-Scale Matched Index of Refraction Flow Facility for LDA Studies Around Complex Geometries," *Exp. Fluids*, **30**, 391 (2001).

19. N. ZUBER, "An Integrated Structure and Scaling Methodology for Severe Accident Technical Issue Resolution," Appendix D, NUREG/CR-5809, U.S. Nuclear Regulatory Commission (1991).

20. J. R. TALLACKSON, "The Thermal Transport Properties of Helium, Helium-Air Mixtures, Water and Tubing Steel Used in the CACHE Program to Compute HTGR Auxiliary Heat Exchanger Performance," ORNL/TM-4931, Oak Ridge National Laboratory (1976).

21. J. P. HOLMAN, *Heat Transfer*. 6th ed. McGraw-Hill, New York (1986).